

Chapter 7

Behavior of Nanomaterials in Soft Soils: A Case Study

Zaid Hameed Majeed and Mohd Raihan Taha

7.1 Introduction

There is a severe shortage of desirable soil especially in developing world due to its extensive demand for domestic and industrial developments. As a consequence, undesirable soil must be looked for as alternative and therefore efforts should be concentrated on making it a useful entity and productive enough in the near future, given the fast depletion of desirable soil in nature (Sariosseiri and Muhunthan 2009).

In general, weak soils have caused problems in buildings, embankments, pavements, etc., and hence its engineering properties need to be enhanced.

Soft soil is a type of problematic soil which can be found in areas with high water content, namely, approaching that of the liquid limit, which results in high settlement potential with low shear strength. The construction of infrastructures, such as road embankments and bridge foundations, on soft soils in many civil engineering projects has prompted the introduction of many approaches for soil treatments.

The design solution may include the expensive option of removal and replacement of the undesirable soils. Another design option includes utilizing ground improvement alternatives such as sand drain, grouting, and chemical stabilization.

Soil stabilization is the technique of increasing the strength and durability while decreasing compressibility, permeability, shrinkage limits, and swelling by using mechanical and/or chemical methods (Calik and Sadoglu 2014). The traditional

Z.H. Majeed (✉)

Department of Civil Engineering, College of Engineering, University of Babylon, Babil, Iraq
e-mail: Eng.zaid.hameed@uobabylon.edu.iq

M.R. Taha

Department of Civil and Structural Engineering, Faculty of Engineering and Built Environment, Universiti Kebangsaan Malaysia (UKM), 43600 Bangi, Selangor, Malaysia
e-mail: dr.mrt@eng.ukm.my

stabilizers such as cement, lime, ash in different sources (fly ash, rice husk ash, and leaf boom ash) have been extensively researched and their stabilization mechanisms have also been discussed extensively (Rahmat and Kinuthia 2011).

During the recent years, there has been a great deal of interest in nanotechnology and nanoparticles (Brar et al. 2009). Some researchers have introduced nanomaterials for use in soil stabilization.

7.2 Soft Soil

Soft soil characteristics include high compressibility, low shear strength, and low permeability. All these characteristics will eventually lead to low bearing capacity and excessive settlement problem. Soft soils are also sensitive and their strength can be reduced by slight disturbances.

According to Kempfert and Gebreselassie (2006), “soft soils” can be defined as clay or silty clay soil which is geologically young and is under a stable condition due its own weight yet has not undergone significant secondary consolidation since its formation. Moreover, the soils are just capable of carrying its own overburden weight and any imposed additional load will result in relatively large deformation.

Clays according to the Unified Soil Classification System (USCS) are fine-grained soils with more than 50 % by weight passing No. 200 US Standard Sieve (0.075 mm) which have much larger surface areas than coarse-grained soils and responsible for the major physical and mechanical differences between coarse-grained soils.

7.2.1 Nanomaterials

Nanotechnology has changed our vision, expectations, and abilities to control the material world (Sobolev et al. 2008). The developments in nanoscience can also have a great impact on the field of construction materials (Pacheco-Torgal and Jalali 2011). Nanotechnology deals with the production and application of physical, chemical, and biological systems at scales ranging from a few nanometers to submicron dimensions, as well as the integration of resulting nanostructures into large systems (Bhushan 2007; Prasad 2014; Prasad et al. 2014, 2016).

Nanomaterials can be metals, ceramics, polymeric materials, or composite materials. Three groups of nanomaterials can be distinguished based on their geometry or shape: quantum well (1 nanosized dimension), quantum wire (2 nanosized dimensions), and quantum dot (3 nanosized dimensions) (Poole and Owens 2003). One of the principal structural units in nanotechnology is quantum dot or nanoparticles, which can be represented as a cluster of tens to thousands of atoms 1–100 nm in diameter (Sobolev and Gutiérrez 2005).

Nanomaterials are poised for widespread use in the construction industry, where they can offer significant advantages for a variety of applications ranging from making more durable concrete to self-cleaning windows (Hosseini et al. 2010; Lee et al. 2010; Givi et al. 2011; Akhnoukh 2013; Ubertini et al. 2014).

Moreover, most properties at the micro scale remain approximately the same as those of the bulk materials. The decrease in one or more geometric dimensions down to the nanoscale completely modifies the behavior of the material. Thus, high surface-to-volume ratio and cation exchange capacity exist at the nanoscale (Olga and Hanna 2014). Nanoparticles interact actively with other particles and solutions, and very minute amounts may lead to considerable effects on the physical and chemical properties of a material. Gravitational force at the nanoscale can be disregarded. Instead, electromagnetic forces are dominant (Mercier et al. 2002).

At nanometer scale, the contacting surfaces between soil particles can be more perfect as the size of particle is smaller. The friction in soil particle at nano scale can change over the class of magnitude (a range of values a designated lower value and an upper value ten times as large) depending on the relative arrangement of the contacting surfaces. Sometimes, the particle movement is restricted in one direction. In other cases the particle rolls or rotates or slides in plane, which can increase shear forces (Falvo and Superfine 2000). In addition, nanoparticles significantly enhance the mechanical properties of different materials, i.e., metals, polymers, ceramic, and concrete composites (Sobolev and Sanchez 2012).

The idea of using nanomaterial to improve soil comes from the inter-particles concept. According to Montesh (2003, 2005) the difference between the particle size contributes to inter-particle filling or interlayer filling, which reduce the void ratio. Moreover, flocculation and dispersion of clay particles can play an important role in hydraulic conductivity. One of the important factors that increase the flocculation is the electrolyte concentration. A small diffuse double layer (DDL) leads to a decrease of electrostatic repulsion, which results to move clay particles toward each other and become flocculation, which causes a increase in hydraulic.

7.3 Materials

7.3.1 Soils Used in the Experimental Work

Three soils were used in this study to evaluate the effects of nanomaterials. Soil samples were obtained from three different locations in Malaysia, shown in Fig. 7.1. Location (A), shown in Fig. 7.2 as S1 is on the Engineering Campus of the Universiti Sains Malaysia, located in Transkrian area is approximately 500 km north of Kuala Lumpur. Location (B), represented by S2, is located in the Sungai Manggis district of the town of Banting, approximately 57 km west of Kuala Lumpur. Location (C), represented by S3, is located in Rengit, Batu Pahat, Johor, approximately 300 km south of Kuala Lumpur. The three soils used were classified

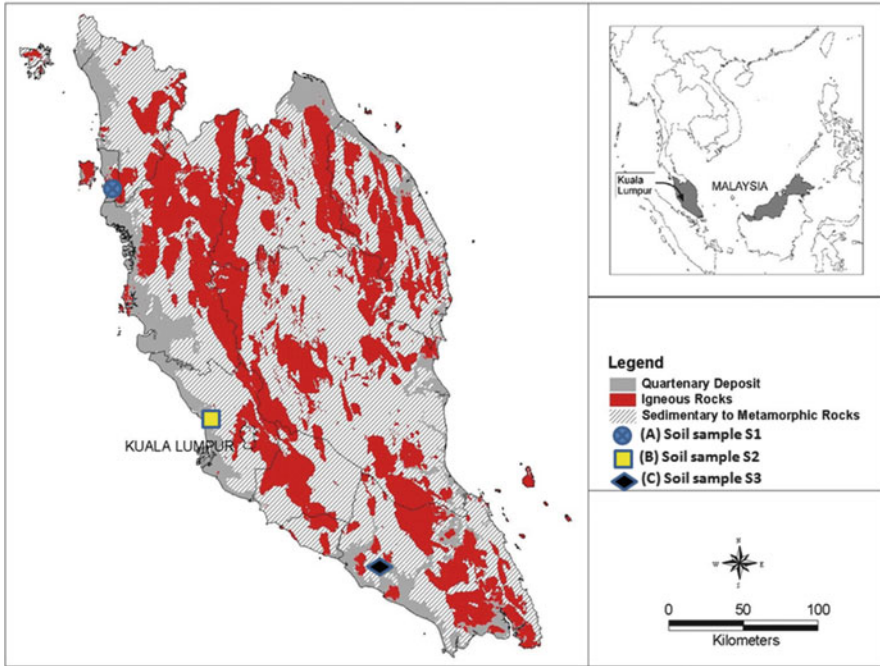


Fig. 7.1 Soil sample collection sites in Malaysia

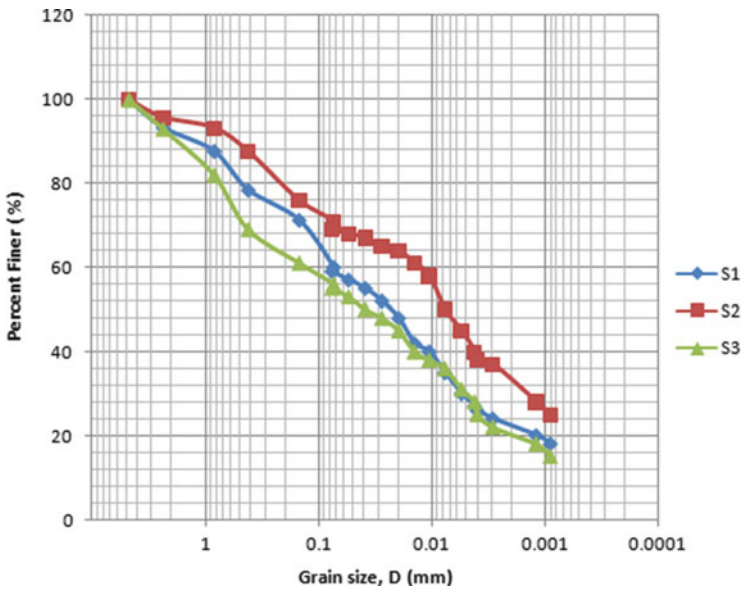


Fig. 7.2 Grain size distributions of the tested soils

Table 7.1 Physical and chemical properties of the soils

| Characteristics | Values and descriptions | | |
|--|-------------------------|-------|-------|
| | S1 | S2 | S3 |
| Natural water content (%) | 35.53 | 43.33 | 29.83 |
| Organic content (%) | 12.17 | 1.31 | 4.88 |
| Specific gravity | 2.42 | 2.75 | 2.49 |
| Ph | 3.24 | 4.25 | 7.50 |
| Clay fraction (%) | 29.8 | 36.2 | 22.3 |
| Silt fraction (%) | 31.3 | 31.3 | 33.2 |
| Sand fraction (%) | 38.9 | 32.5 | 44.5 |
| Liquid limit index (%) | 46.35 | 50.61 | 52.40 |
| Plasticity index (%) | 18.25 | 25.61 | 21.1 |
| Linear shrinkage (%) | 11.07 | 8.24 | 8.96 |
| Unified soil classification (USCS) | OL | CH | MH |
| Optimum water content (%) | 21.60 | 24.80 | 17.30 |
| Maximum dry unit weight (kN/m ³) | 14.44 | 15.68 | 17.46 |
| Unconfined compressive strength (kN/m ²) | 90.0 | 43.0 | 65.0 |
| <i>Chemical composition</i> | | | |
| SiO ₂ (%) | 61.72 | 57.03 | 56.23 |
| Al ₂ O ₃ (%) | 17.53 | 23.63 | 25.55 |
| Fe ₂ O ₃ (%) | 3.61 | 7.33 | 4.68 |
| MgO (%) | 1.16 | 0.73 | 0.40 |
| CaO (%) | 0.06 | 0.04 | 0.25 |
| TiO ₂ (%) | 0.89 | 1.80 | 1.03 |
| Na ₂ O (%) | 0.40 | 0.31 | 0.04 |
| K ₂ O (%) | 2.92 | 2.51 | 0.37 |
| Others | 11.71 | 5.31 | 6.57 |

according to Unified Soil Classification System (ASTM 2005), respectively, as organic silty soil (OL), clay high plasticity soil (CH), and high plasticity silt soil (MH) as shown in Table 7.1.

All soil samples were disturbed samples. They were collected from a depth of 0–0.75 m below ground level by big plastic bag. After transportation to the laboratory of soil mechanics in UKM University, the soil samples were air-dried and then oven-dried at 100 ± 5 °C over 24 h. Thereafter, pulverization machine was used to crush the soil with proper mixing to obtain uniform soil samples. Thereafter, the soil samples were stored in big plastic drums. Table 7.1 presents the physical and chemical properties of the three soils.

7.3.2 Nanomaterials

Three types of nano materials were used in this study, i.e., nano-copper, nano-alumina, and nano-magnesium. Some properties of the nanomaterials are discussed below.

1. Nano-Copper

The copper oxide nanopowder used in this study has a purity of 99.99 %, and supplied by Inframat Advanced Materials, Manchester, CT, USA. The copper oxide nanopowder is insoluble in water. It dissolves slowly in alcohol or ammonia solution. It is also soluble in dilute acids, NH_4Cl , $(\text{NH}_4)_2\text{CO}_3$, potassium cyanide solution under high temperature. Nano-copper oxide is a widely used material and been applied as catalyst for superconducting materials, thermoelectric materials, sensing materials, glass, ceramics, etc. A scanning electronic microscope image (SEM) for copper oxide nanopowder is shown in Fig. 7.3 and an X-ray diffraction (XRD) patterns for nano-copper showed in Fig. 7.4. The average particle diameter for copper oxide nanopowder is about 100 nm. The other properties for copper oxide nanopowder are shown in Table 7.2.

2. Nano-Alumina

The nano-alumina material used in this study is Ultrapure Gamma-Alumina ($\gamma\text{-Al}_2\text{O}_3$) powder with purity of 99.99 %, with high activity and low melting temperature. The nanomaterial has a large surface area and high catalytic activity. It can be made into micro porous spherical structure or honeycomb

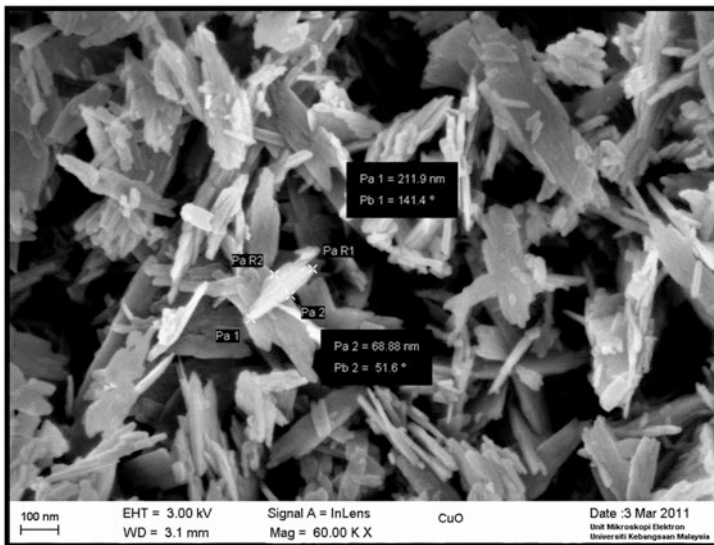


Fig. 7.3 Scanning electronic microscope image for copper oxide nanopowder

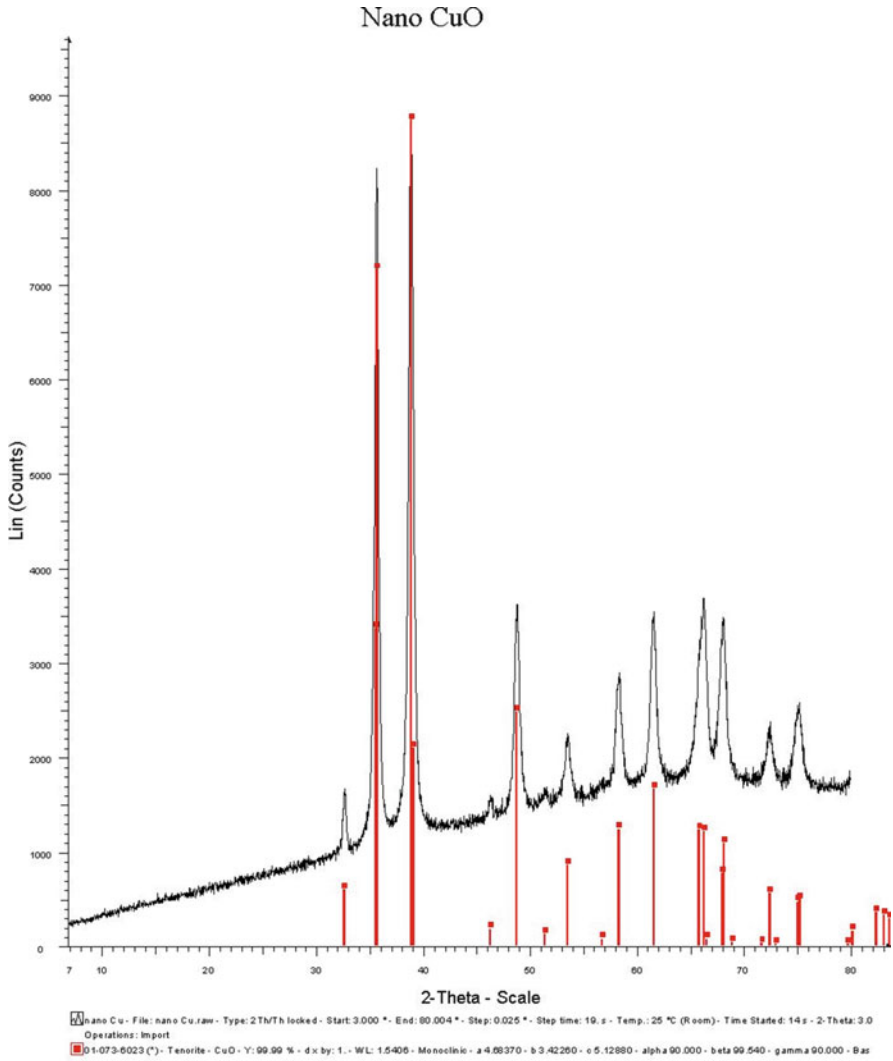


Fig. 7.4 X-ray diffraction (XRD) patterns for copper oxide nanopowder

structure of catalytic materials. These kinds of structures can be excellent catalyst carriers. If used as industrial catalysts, they will be the main materials for petroleum refining, petrochemical and automotive exhaust purification. This powder was supplied by Inframat Advanced Materials, Manchester, CT, USA. A scanning electronic microscope image (SEM) shows the nano-alumina powder in Fig. 7.5, moreover the XRD patterns of nano-alumina shown in Fig. 7.6. The particle size of gamma phase nano-alumina ranged from 20 to 50 nm and the other general properties of nano-alumina powder are shown in Table 7.3.

Table 7.2 Properties of copper oxide (CuO) nano powders

| Property | Value |
|---------------------------------------|--------------------------|
| Formula | CuO |
| Particle density (g/cm ³) | 6.3–6.49 |
| Surface area (m ² /g) | N/A |
| Average particle size (nm) | 100 |
| Solubility in water (%) | Insoluble |
| Melting point (°C) | 1326 |
| <i>Composition</i> | |
| Al ₂ O ₃ | N/A |
| Cu | 99.99 % |
| Appearance and odor | Black powder Odorless |
| Crystal structure | N/A |

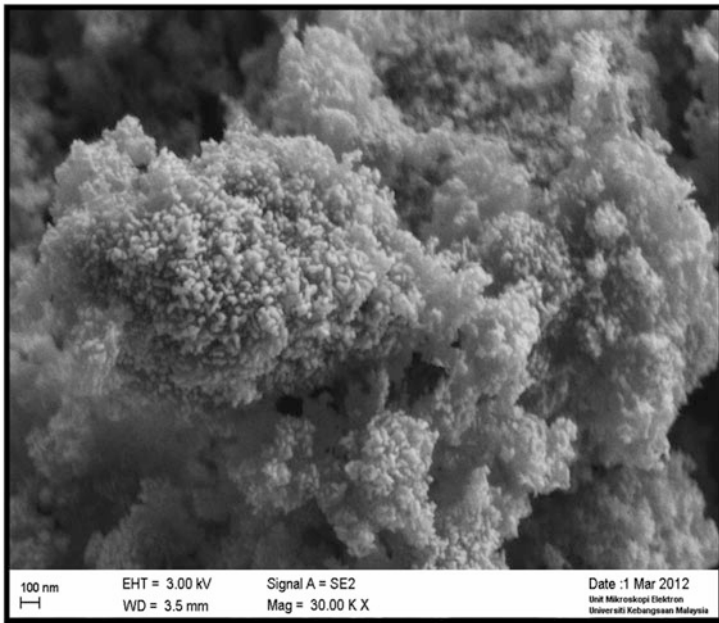


Fig. 7.5 Scanning electronic microscope image for nano alumina powder

3. Nano-Magnesium

The nano-magnesium oxide (N-MgO) of high purity was supplied by Inframat Advanced Materials Company, Manchester, USA. The specifications and all the information provided by the company are shown in Table 7.4. Figures 7.7 and 7.8 respectively show the scanning electronic microscope (SEM) and XRD patterns for the nano-magnesium. The average particles size was 100 nm.

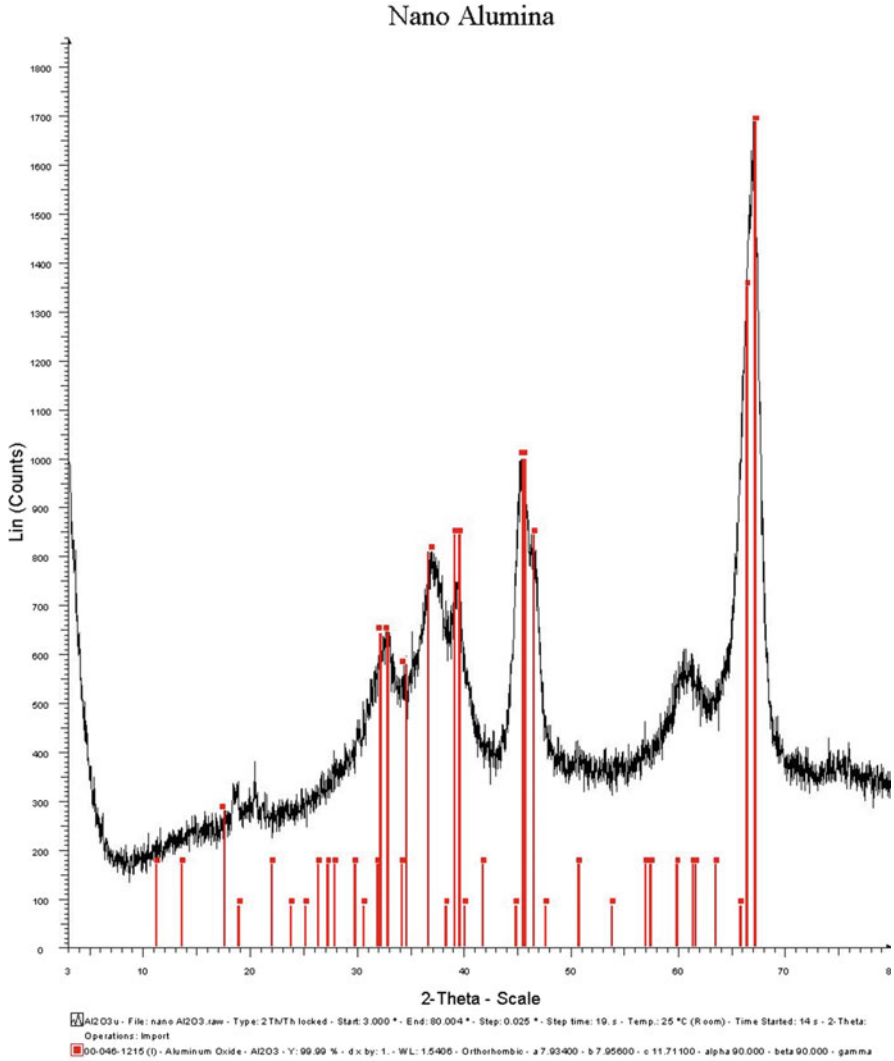


Fig. 7.6 X-ray diffraction (XRD) patterns for nano-alumina nanopowder

7.4 Preparation of Soil: Nanomaterials Mixtures

The amount of nanomaterial required for each specimen was determined by multiplying the nanomaterial percentage by the total dry weight of the soil. The mixture proportions are listed in detail in Table 7.5. Different amounts of the different nanomaterials used.

Taha and Taha (2012) have reported that the best way to obtain homogeneous samples is to mix the nanomaterials with the dry in two stages. This procedure was

Table 7.3 Properties of gamma aluminum oxide (alumina Al_2O_3) nano powders

| Property | Value |
|---|--------------------------------|
| Formula | Al_2O_3 |
| Particle density (g/cm^3) | 3.6 |
| Surface area (m^2/g) | >150 |
| Average particle size (nm) | 20–50 |
| Solubility in water (%) | Insoluble |
| <i>Composition</i> | |
| Al_2O_3 | $\geq 99.99\%$ |
| Appearance and odor | White to off-white Odorless |
| Crystal structure | Transitional gamma |

Table 7.4 Properties of magnesium oxide (magnesium MgO) nano powders

| Property | Value |
|---|----------------------------|
| Formula | MgO |
| Particle density (g/cm^3) | 3.6 |
| Surface area (m^2/g) | >50 |
| Average particle size (nm) | 100 |
| <i>Composition</i> | |
| MgO | $\geq 99.90\%$ |
| Appearance and odor | White to pearl Odorless |
| Crystal structure | Transitional gamma |

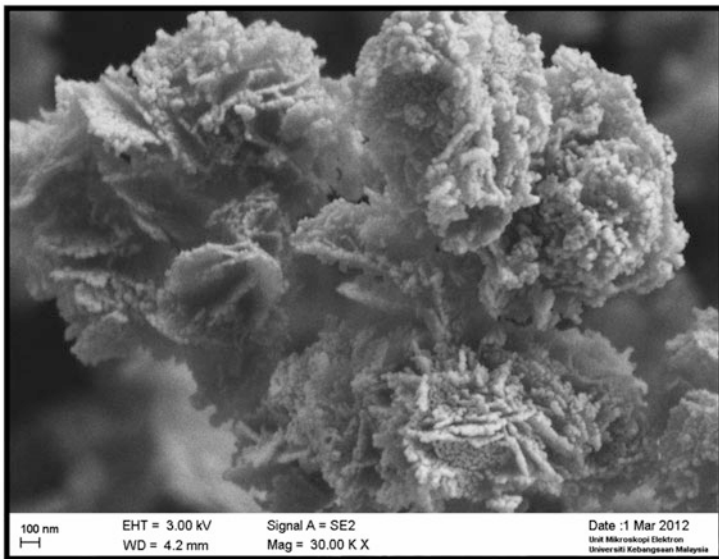


Fig. 7.7 Scanning electronic microscope image of nano-magnesium

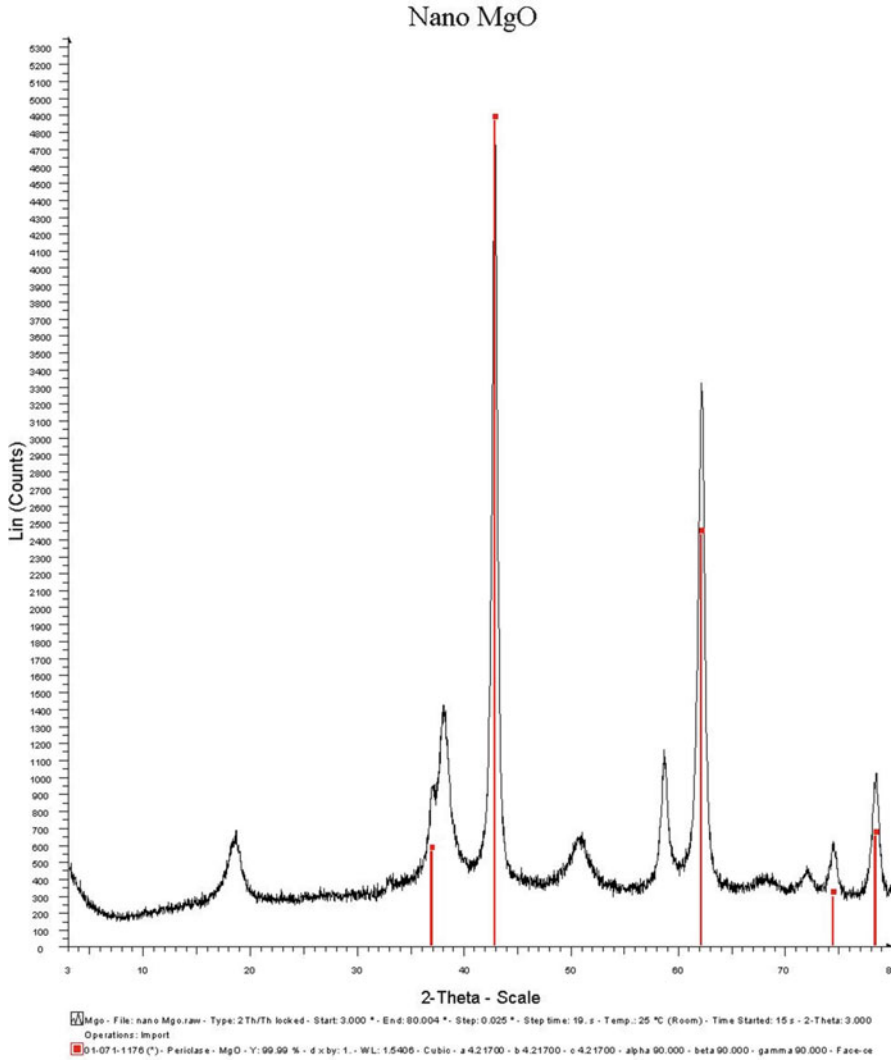


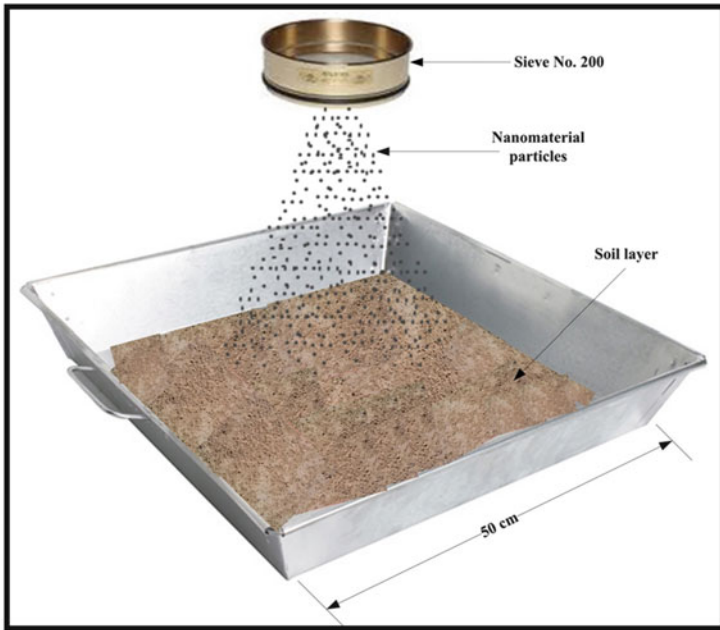
Fig. 7.8 X-ray diffraction (XRD) patterns for nano-magnesium nanopowder

adopted in current study. First, premix or hand mixed the quantity of soil was divided into ten portions and each portion was spread in a square pan (50 × 50 cm), then the required amount of nanomaterial was sprayed using sieve number 200 as shown in Fig. 7.9.

In the second stage, the resulting mixtures were mixed together as shown in Fig. 7.10 for at least 3 h using a horizontal cylindrical mixer to ensure that the samples were homogeneous. In order to avoid the segregation problem, the soil-nanomaterial mixture was mixed with the required water content directly then the

Table 7.5 Mix proportions for nanomaterials (by % weight of dry soil)

| Nano-copper (%) | Nano-alumina (%) | Nano-magnesium (%) |
|-----------------|------------------|--------------------|
| 0.0 | 0.0 | 0.0 |
| 0.3 | 0.05 | 0.1 |
| 0.5 | 0.075 | 0.2 |
| 0.7 | 0.1 | 0.3 |
| 0.8 | 0.15 | 0.35 |
| 1.0 | 0.2 | 0.4 |

**Fig. 7.9** Spraying of nanomaterial on the soil layer

entire mixture was placed in a sealed plastic bag and left for 24 h for hydration. This mixing method was repeated every time needs to prepare a new mixture. This procedure was found to be the best method to obtain homogeneous samples since homogeneous color was obtained after compaction (Fig. 7.11). However, proper care was taken to prepare homogeneous mixtures at each stage.

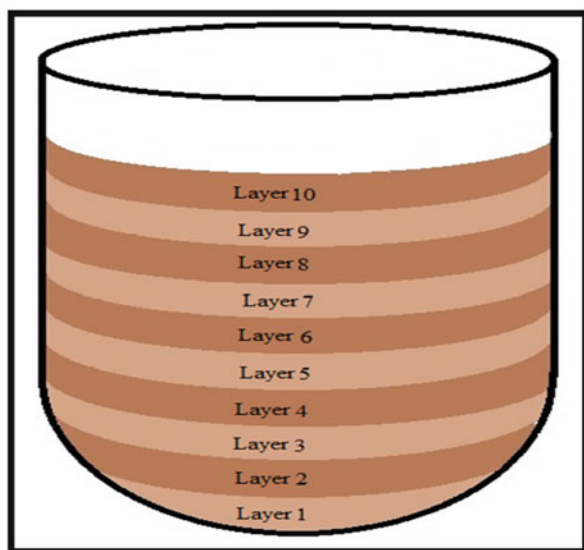


Fig. 7.10 Mixing all quantity in a pot

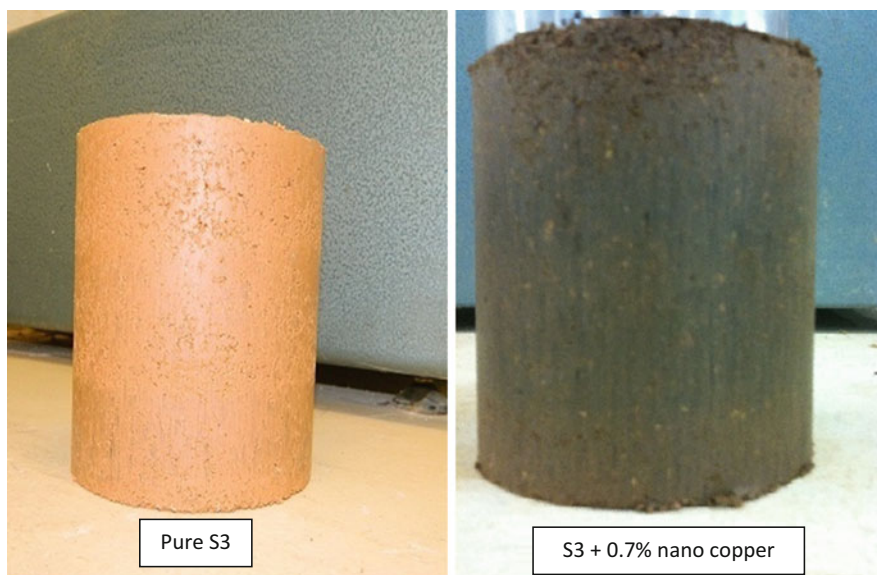


Fig. 7.11 The homogeneous color of samples obtain after compaction

7.5 Experimental Laboratory Test Program

7.5.1 The pH Test

In this work, the electrometric method (BS 1377: part 3: 1990: clause 9) was utilized to determine the pH value of soil suspension in water and is considered to be the most accurate method. This method requires a soil–water ratio of 1:2.5 and can be obtained by passing 30 g soil through a 2 mm sieve and diluted with 75 ml distilled water for at least 8 h. Figure 7.12 shows the pH meter device with samples preparation procedures which used in this test.

7.5.2 Atterberg Limits Test

The Atterberg limits (i.e., the liquid limit, the plastic limit, and the plasticity index) of each of the natural and stabilized soil samples were determined in accordance with BS 1377, part 2, 1990. The liquid limit tests were performed using a penetration cone assembly, which consisted of a stainless steel cone with a cone angle of $30^\circ \pm 1^\circ$. The plastic limit tests were performed using a manual method. Each sample was rolled at a sufficient pressure on a glass plate to form a thread with a uniform diameter of 3.2 mm along the full length of the sample. The plasticity index



Fig. 7.12 Sample preparation procedures for pH test

was calculated as the difference between the water contents at the liquid and plastic limits.

7.5.3 *Fourier Transform Infrared Spectroscopy*

The Fourier Transform Infrared (FT-IR) model PerkinElmer System 2000 was used to analyze the possible chemical bonding existing in the untreated and treated soil. Each 25–30 g sample was dried in a microwave oven at the 100 °C for 30 min. The sample was subjected to light grinding in a mortar and the sample was then filtered through a coarse sieve to remove large structures. Approximately 5 g of each filtered sample was ground, passed through a 0.074 mm sieve, and then stored in closed glass vials pending further examination.

The specimens were introduced as pellets prepared from powder mixed with KBr and spectra were recorded in the range 400–4000 cm^{-1} . KBr powder pellets were used as a background.

7.5.4 *X-ray Diffraction*

X-ray diffraction (XRD) analysis of untreated and treated soft soil was carried out using a BRUKER AXS D8 ADVANCE machine as shown in Fig. 7.13. The XRD patterns were obtained using a Cu-K α ($k = 1.5148 \text{ \AA}$) X-ray tube with an input voltage of 40 kV and a current of 40 mA. A continuous scan mode and scan rate of 2° per minute was selected. Air-dried powdered samples of treated and untreated soil samples were used as shown in Fig. 7.14. Soil mineralogy obtained from the test provides the basis for understanding the basic mechanisms of chemical stabilization.

7.5.5 *Field-Emission Scanning Electron Microscope*

Field-emission scanning electron microscope (FESEM) was conducted to disclose the morphology of the native materials and to observe the morphology of the materials after mixing and curing. The change in the soil aggregation and formation of new material can be observed by this analysis, knowing that same specimens were used to perform EDX analysis mentioned previously. Figure 7.15 shows the instrument employed for FESEM and EDX analysis.



Fig. 7.13 The XRD instrument



Fig. 7.14 Sample preparation procedures for XRD test

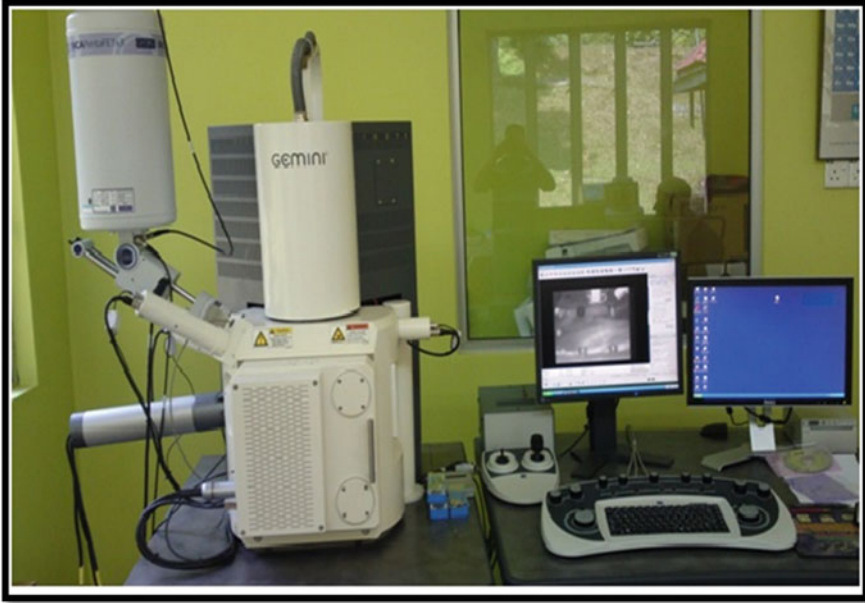


Fig. 7.15 Instrument employed for FESEM and EDX analysis

7.5.6 X-ray Fluorescence Analysis

X-ray fluorescence (XRF) analysis was conducted for the native materials, i.e., virgin soil, and nanomaterials (nano-copper, nano-alumina, and nano-magnesium) to obtain their chemical compositions and to create a perception about the expected reactants. The soil was milled sieved on 425 μm before XRF analysis. For each material, a small compressed disk specimen was prepared as shown in Fig. 7.16. Figure 7.17 presents the machine employed for XRF analysis.

7.6 Physicochemical Aspects of Nanomaterials Treatment

7.6.1 The pH Test

The effect of nanomaterials on pH value were investigated to evaluate the chemical reactions after mixing nanomaterials with the tested soils. The influence of nano-copper, nano-alumina, and nano-magnesium on the pH of different soil samples is shown in Figs. 7.18, 7.19, and 7.20, respectively. The test results showed that the pH of the stabilized soil samples increased with increasing nanomaterials percentage. All nanomaterials had pH higher than the control soils.



Fig. 7.16 Specimens prepared for XRF analysis



Fig. 7.17 XRF equipment used in this study

Fig. 7.18 pH for different nano-copper percentages after mixing with different soils

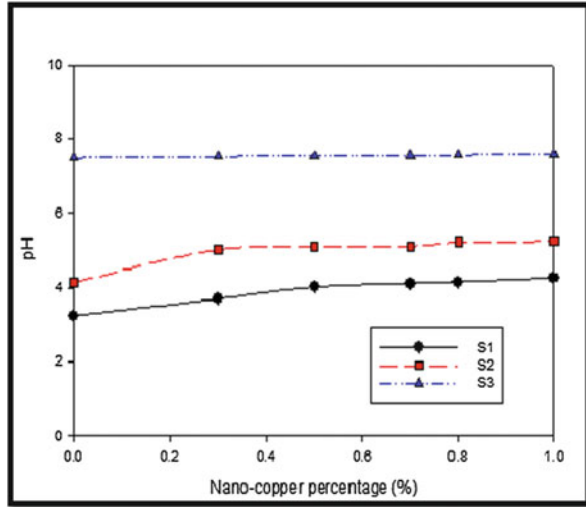
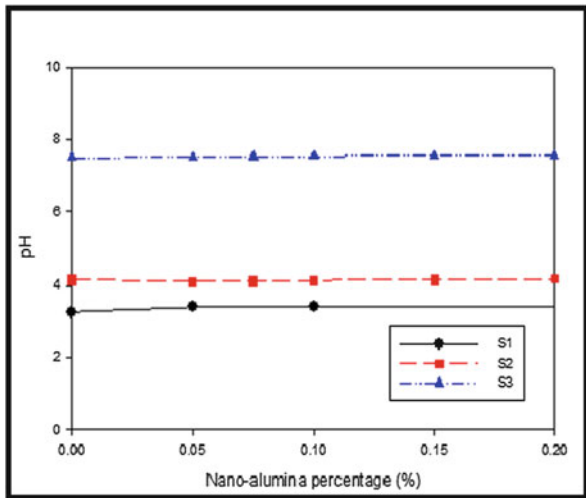
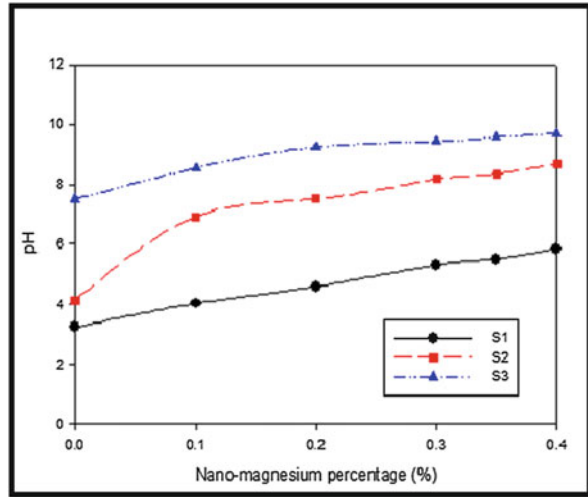


Fig. 7.19 pH for different nano-alumina percentages after mixing with different soils

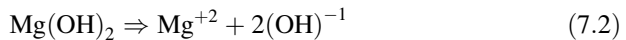
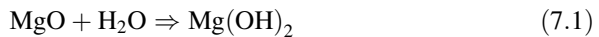


The treatment of the samples with nanomaterial content changed the pH, and the value increased with increasing nanomaterial content for all samples. The pH value of S1, S2, and S3 soil samples treated with nano-copper and nano-alumina increased when the percentage of additive increased due to low pH values of S1, S2, and S3 soil samples (3.24, 4.25, and 7.50, respectively). Moreover, the increase in pH value for samples treated with nano-copper was higher than nano-alumina because the additive content for nano-copper was greater than nano-alumina, also these changes can be attributed to the properties associated with the original soil sourced from the tropical region. Due to climate effect and the origin of the soil is acidic in nature.

Fig. 7.20 pH for different nano-magnesium percentages after mixing with different soils



Moreover, the chemical action of nanomaterials by formation new hydroxide as nano-magnesium, which is the formation of $Mg(OH)_2$ elucidated above, is followed by the ionization process inducing liberation of hydroxyl ions $(OH)^{-1}$ which is possibly the reason behind the increase the pH value. The following chemical equations can explain the formation and ionization processes (Mo et al. 2012; Shand 2006; Zhang et al. 2011).



However, the increase in pH value is also one of the indications of increasing the cementation of colloidal particles (Muhunthan et al. 2008).

7.6.2 X-ray Diffraction Analyses

Diffraction analysis of stabilized soil is important to determine the changes that occur in the mineralogical phase reactions. These reactions depend on the chemical and mineralogical composition of each soil and additive. Figures 7.21, 7.22, and 7.23 respectively show the XRD patterns for untreated soil samples S1, S2 and S3. As shown in Figs. 7.21, 7.22, and 7.23, quartz and kaolinite are clearly appearing in the untreated soft soils. In this case, the XRD peaks of quartz are significantly larger than the peaks of other minerals because quartz is better X-ray-scattered than other compounds. The peak located at 2-Theta 26.67° was identified as quartz. The d-spacing shows the change in crystals of materials. It is defined as the distance between two successive structure units and is dependent on the type of the

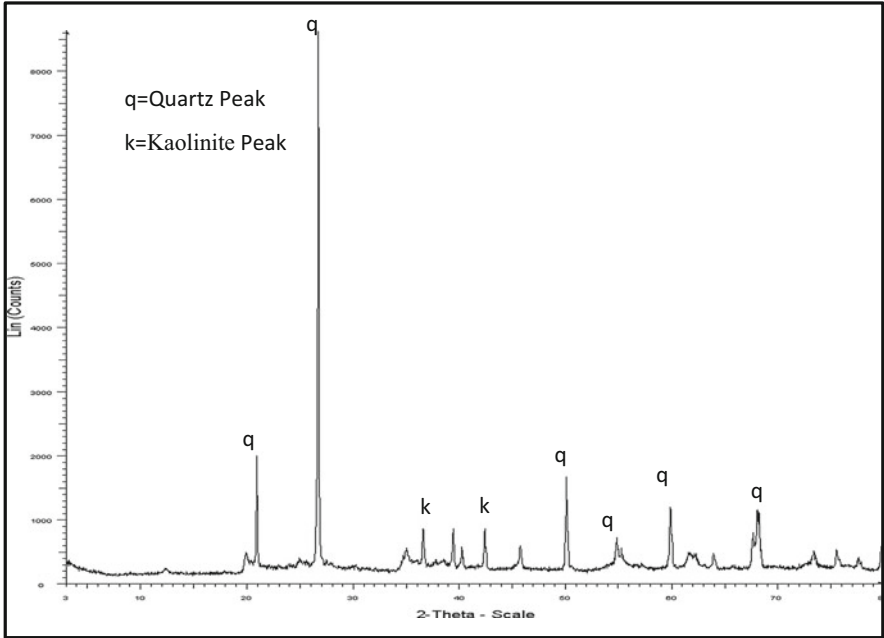


Fig. 7.21 XRD patterns for unstabilized soil sample S1

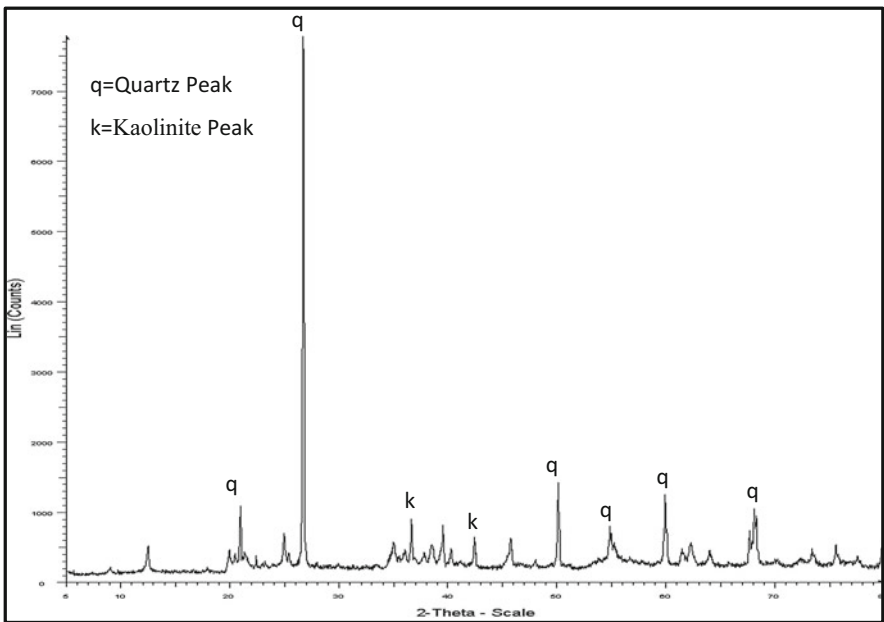


Fig. 7.22 XRD patterns for unstabilized soil sample S2

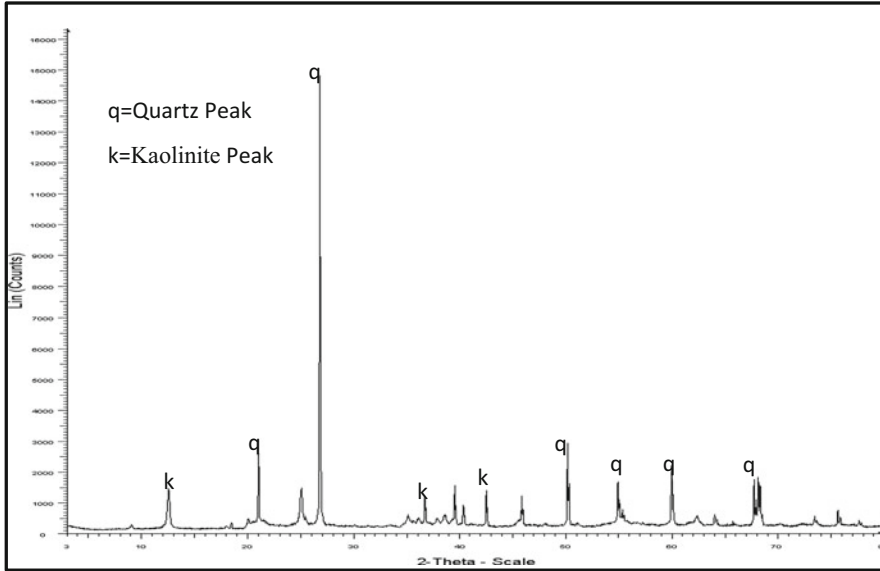


Fig. 7.23 XRD patterns for unstabilized soil sample S3

Table 7.6 The d-spacing values of different soils obtained for the quartz peak

| Soil no. | Original soil (Å) | Nano-copper (Å) | Nano-alumina (Å) | Nano-magnesium (Å) |
|----------|-------------------|-----------------|------------------|--------------------|
| S1 | 3.3421 | 3.33562 | 3.3218 | 3.32854 |
| S2 | 3.34305 | 3.34317 | 3.32187 | 3.33656 |
| S3 | 3.33464 | 3.32328 | 3.31686 | 3.32996 |

Table 7.7 The intensity values of different soils obtained for the quartz peak

| Soil no. | Original soil (Count) | Nano-copper (Count) | Nano-alumina (Count) | Nano-magnesium (Count) |
|----------|-----------------------|---------------------|----------------------|------------------------|
| S1 | 8675 | 10262 | 11910 | 10911 |
| S2 | 7816 | 9170 | 7536 | 8521 |
| S3 | 5426 | 6161 | 6233 | 5884 |

exchangeable cation, the solution composition, and the clay composition (Amorim et al. 2007). The d-spacing for the soils before and after adding the nanomaterials are shown in Table 7.6. For the sake of simplicity, only the optimum nano percentages and the highest quartz peaks for each soil are shown. From Table 7.6, it can be seen that the d-spacing reduced slightly which reflects the effect of the added nanomaterials. To provide further evidence of the chemical reactions of the soils-nanomaterials under consideration, the intensity values for the optimum nanomaterials content and the highest quartz peaks for each soil are tabulated in Table 7.7. It can be seen from the data in Table 7.7 that the intensity increased in all the stabilized soils. This intensity increment again emphasized the effect of the added nanomaterials.

As mentioned before, the XRD patterns of nanomaterials-treated soils reveal several new peaks as compared to the untreated soils. This result may be explained by the fact that chemical action of the nanomaterials agreed with the results obtained from the strength and compressibility test.

7.6.3 Fourier Transform-Infrared Analysis

FT-IR spectroscopy is an important tool for investigating structural changes in soil-stabilized surface. Previous studies used FT-IR to examine the effect of treatment on the changes in the chemical bonds in the stabilizer surface (Millogo et al. 2008).

FT-IR was performed to evaluate the mineral soil bands, which were tested between 400 and 4000 cm^{-1} (Du et al. 2008). The representative FT-IR spectra of the soil samples without nanomaterials are shown in Figs. 7.24, 7.25, and 7.26. The observed wavenumber from all the spectra are given in Tables 7.8, 7.9, and 7.10 along with their corresponding mineral names.

The FT-IR spectra indicated quartz and kaolinite as major constituents and other minerals as minor constituents. Strong bands between 3696 and 3622 cm^{-1} indicated the possibility of hydroxyl linkage. However, a broad absorption band at 3431 cm^{-1} in the clay spectrum suggests the possibility of water hydration in the adsorbent. The bands at 3696, 3625, 1033, and 914 cm^{-1} showed the presence of kaolinite (Manoharan et al. 2012). Kaolinite, the major constituent of clays, provides sharp absorption bands in the 3700–3600 cm^{-1} region. Quartz is a nonclay mineral that is common and invariably present in all samples. Si–O bonds are the

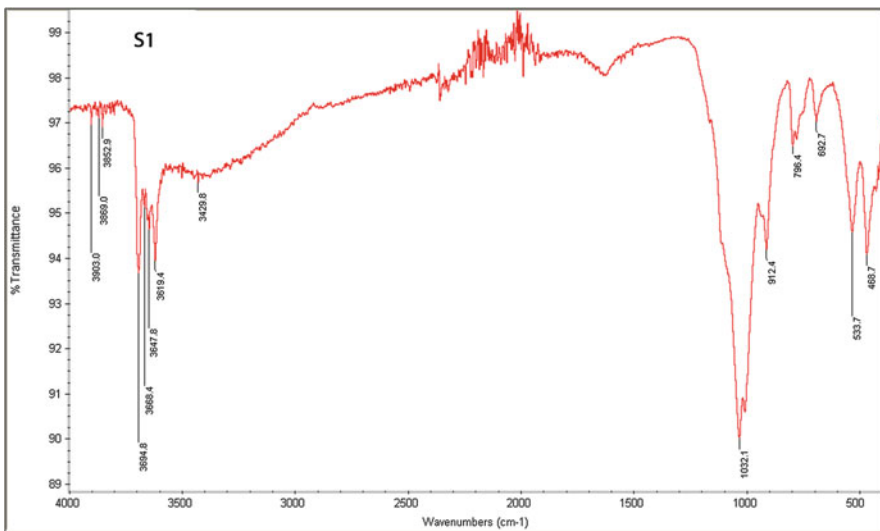


Fig. 7.24 Fourier-transform infrared (FT-IR) spectra of original soil S1

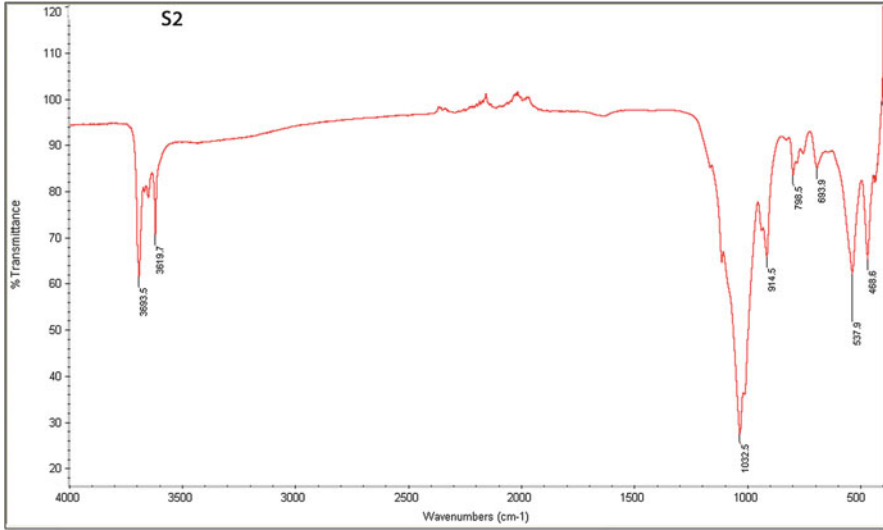


Fig. 7.25 Fourier-transform infrared (FT-IR) spectra of original soil S2

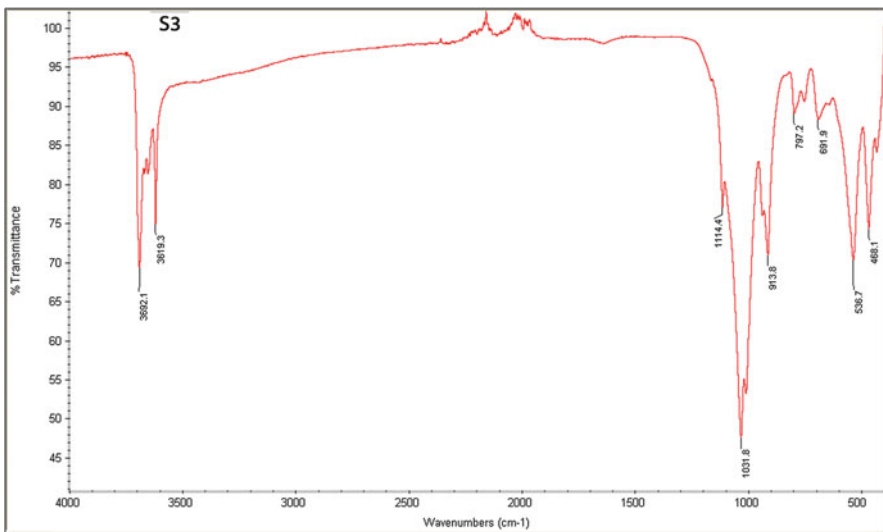


Fig. 7.26 Fourier-transform infrared (FT-IR) spectra of original soil S3

strongest in the silicate structure and can be readily recognized in the infrared spectra of such minerals. The presence of quartz in the samples correspond to Si–O–Si asymmetrical bending vibrations in the $461\text{--}467\text{ cm}^{-1}$ region (Manoharan et al. 2012). The strong absorption band at 692 cm^{-1} correspond the Si–O symmetrical bending vibration of quartz. The absorption bands at $779\text{--}792\text{ cm}^{-1}$ corresponded to Si–O symmetrical stretching vibrations, whereas those at 1082

Table 7.8 FT-IR spectra (cm^{-1}) data with their corresponding tentative assignments for soil samples without nanomaterial treatment

| S1 | S2 | S3 | Tentative assignment | Mineral |
|------|------|------|--|-----------------|
| 3694 | 3693 | 3692 | In-plane degenerated vibration of the water molecule | Kaolinite |
| 3619 | 3619 | 3619 | OH stretching of inner-surface hydroxyl groups | Kaolinite |
| 3429 | – | – | H–O–H stretching of water molecules | Montmorillonite |
| – | – | 1114 | Si–O stretching (longitudinal mode) | Quartz |
| 1032 | 1032 | 1031 | Si–O stretching clay mineral | Kaolinite |
| 912 | 914 | 913 | Al_2O –H deformation | Kaolinite |
| 796 | 798 | 797 | Si–O stretching | Quartz |
| 692 | 693 | 691 | Si–O stretching | Quartz |
| 533 | 537 | 536 | Si–O–Al (or) Fe_2O_3 | Hematite |
| 468 | 468 | 468 | Si–O–Si bending | Quartz |

Table 7.9 FT-IR spectra (cm^{-1}) data with their corresponding tentative assignments for soil samples with nanomaterial treatment

| S1 with | | | S2 with | | | Tentative assignment | Mineral |
|---------|----------------------------|-------|---------|----------------------------|-------|--|-----------------|
| N-Cu | N- Al_2O_3 | N-MgO | N-Cu | N- Al_2O_3 | N-MgO | | |
| 3695 | 3694 | 3695 | 3692 | 3691 | 3691 | In-plane degenerated vibration of the water molecule | Kaolinite |
| 3620 | 3620 | 3619 | 3619 | 3651 | 3651 | OH stretching of inner-surface hydroxyl groups | Kaolinite |
| 3397 | 3382 | 3382 | 3415 | 3422 | 3619 | H–O–H stretching of water molecules | Montmorillonite |
| – | – | – | – | – | 3404 | H–O–H stretching of water molecules | Montmorillonite |
| 1640 | 1630 | 1640 | 1642 | 1640 | 1644 | H–O–H stretching | Illite |
| – | – | – | – | 1114 | – | Si–O stretching (longitudinal mode) | Quartz |
| 1030 | 1029 | 1030 | 1031 | 1029 | 1030 | Si–O stretching of clay mineral | Kaolinite |
| 914 | 912 | 913 | 914 | 913 | 913 | Al_2O –H deformation | Kaolinite |
| 795 | 778 | 795 | 798 | 797 | 797 | Si–O stretching | Quartz |
| 691 | 692 | 691 | – | 692 | 692 | Si–O stretching | Quartz |
| 533 | 530 | 532 | 534 | 533 | 534 | Si–O–Al (or) Fe_2O_3 | Hematite |
| 468 | 463 | 464 | 465 | 465 | 467 | Si–O–Si bending | Quartz |

and 1123 cm^{-1} corresponded to Si–O a symmetrical stretching vibrations (Bertaux et al. 1998). Illite and kaolinite are common main clay minerals in soils and natural aerosols. The observed strong absorption frequencies in the $1620\text{--}1646\text{ cm}^{-1}$ region in the clay spectrum suggests the possibility of water hydration in the adsorbent (Gritco et al. 2005). The broad absorption band at 1032 cm^{-1} corresponded to the Si–O stretching of kaolinite which is a clay mineral (Manoharan et al. 2012). The very weak peak at 915 cm^{-1} is due to the Al_2O –H

Table 7.10 FT-IR spectra (cm^{-1}) data with their corresponding tentative assignments for soil samples with nanomaterial treatment

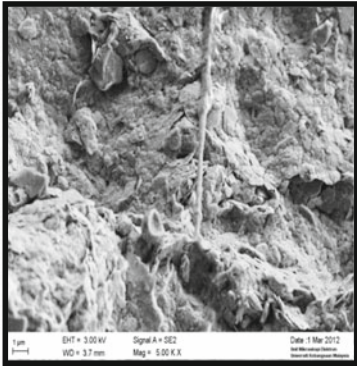
| S3 with | | | Tentative assignment | Mineral |
|---------|----------------------------|-------|--|-----------------|
| N-Cu | N- Al_2O_3 | N-MgO | | |
| 3690 | 3691 | 3690 | In-plane degenerated vibration of the water molecule | Kaolinite |
| 3651 | 3652 | 3651 | O–H stretching of inner hydroxyl group | Kaolinite |
| 3619 | 3619 | 3619 | H–O–H stretching of water molecules | Montmorillonite |
| 3404 | 3413 | 3397 | H–O–H stretching of water molecules | Montmorillonite |
| 2117 | 2114 | – | – | Quartz |
| 1641 | 1640 | 1642 | H–O–H stretching | Illite |
| 1114 | 1114 | 1114 | Si–O stretching (longitudinal mode) | Quartz |
| 1029 | 1030 | 1029 | Si–O stretching clay mineral | Kaolinite |
| 1007 | 1007 | 1006 | In-plane Si–O stretching | Kaolinite |
| 912 | 912 | 912 | Al_2O_3 O–H deformation | Kaolinite |
| 796 | 796 | 796 | Si–O stretching | Quartz |
| 689 | 691 | 690 | Si–O stretching | Quartz |
| 534 | 534 | 534 | Si–O–Al (or) Fe_2O_3 | Hematite |
| 466 | 466 | 466 | Si–O–Si bending | Quartz |

deformation of kaolinite. The strong absorption band at 533 cm^{-1} corresponded to the stretching vibration of Si–O–Al (or) Fe_2O_3 in the presence of hematite (Manoharan et al. 2012).

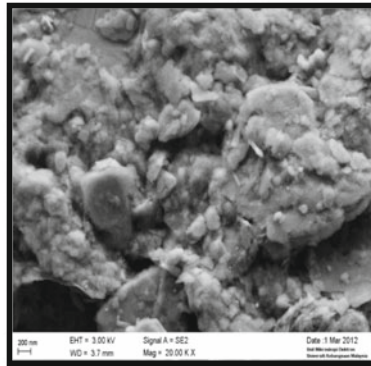
The FT-IR analysis was performed on treated and untreated soft soil to investigate their functional groups. There is a clear difference in spectra observed in the FT-IR results of treated and untreated samples. The presence of the functional groups of nanomaterials in the soil indicates the possible formation of ionic bonding between the clay mineral lattices and the nanomaterial functional groups, as well as the existence of nanomaterials in the interlayer spacing of soil minerals. These changes were probably caused by the action of stabilizer on the clay structure. In addition, the additional spectra observed in the FT-IR results of nanomaterials-treated soil confirm the presence of new functional groups such as Illite (1644 cm^{-1}) and the kaolinite (1029 cm^{-1}). The presence of the functional groups of nanomaterials-treated soil confirms the formation of ionic bonding between the clay mineral lattices and the nanomaterials functional groups and also the existence of nanomaterials in the interlayer spacing of clay minerals.

7.6.4 Scanning Electron Micrographs (SEM) Observations

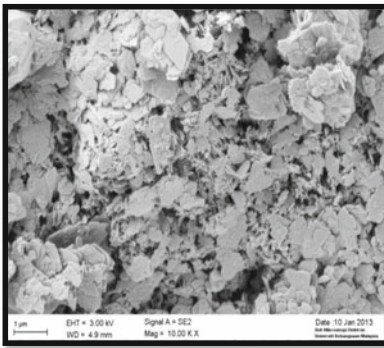
The changes of microstructural and microstructural development of soils due to nano-copper, nano-alumina, and nano-magnesium addition play a significant role in the geotechnical properties and the mechanical behavior of these stabilized soils. Figure 7.27a, b illustrate the SEM-micrograph of natural untreated soil S1. The



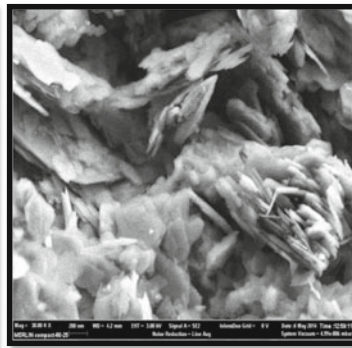
(a) SEM micrograph of S1@ Mag= 5.00 KX



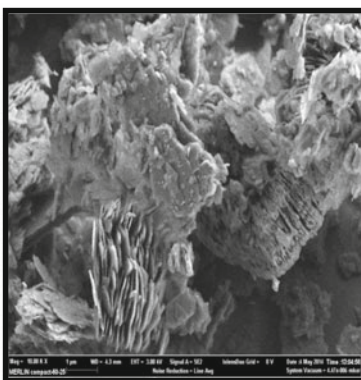
(b) SEM micrograph of S1@ Mag= 20.00KX



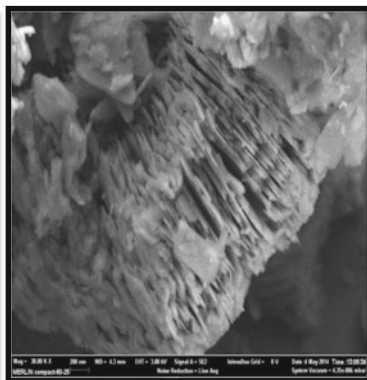
(c) SEM micrograph of S2@ Mag= 10.00 KX



(d) SEM micrograph of S2@ Mag= 30.00 KX



(e) SEM micrograph of S3@ Mag= 10.00 KX



(f) SEM micrograph of S3@ Mag= 30.00 KX

Fig. 7.27 SEM micrograph of the tree natural, untreated soil samples at different magnification. (a) SEM micrograph of S1@ Mag = 5.00 KX. (b) SEM micrograph of S1@ Mag = 20.00 KX. (c) SEM micrograph of S2@ Mag = 10.00 KX. (d) SEM micrograph of S2@ Mag = 30.00 KX. (e) SEM micrograph of S3@ Mag = 10.00 KX. (f) SEM micrograph of S3@ Mag = 30.00 KX

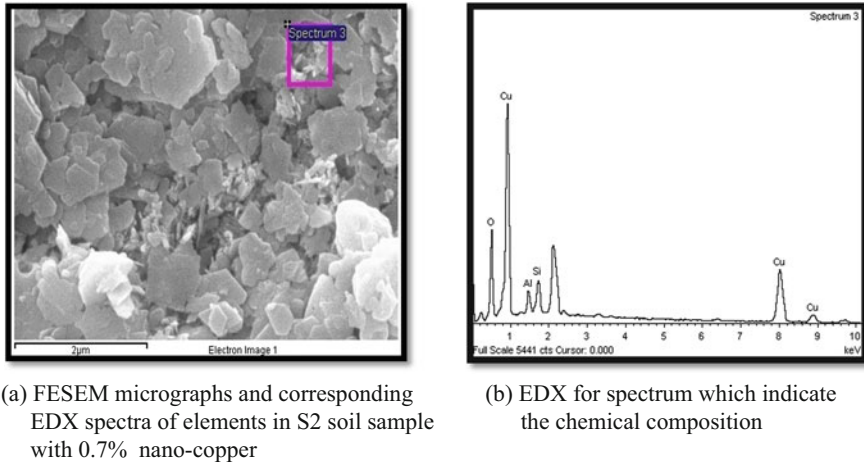
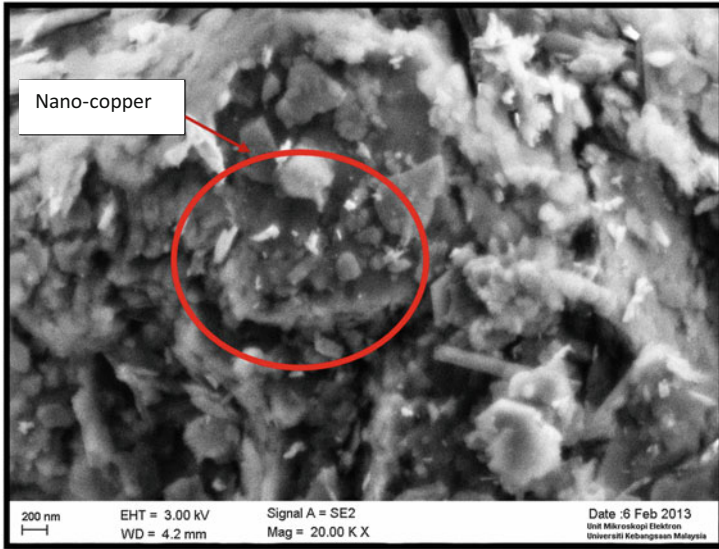


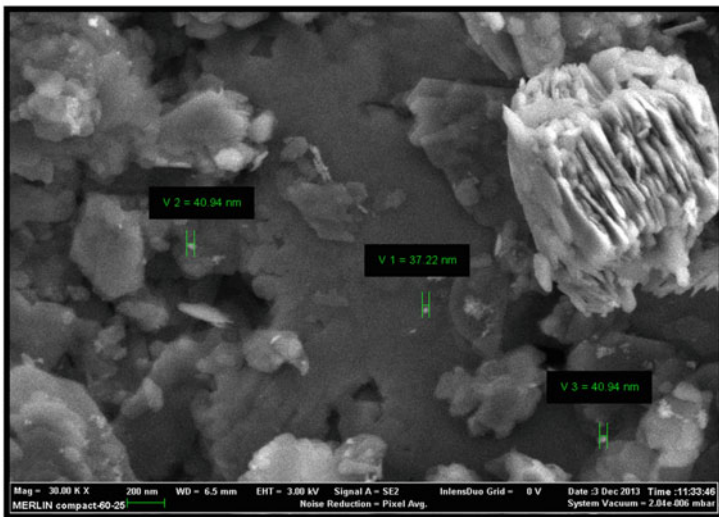
Fig. 7.28 Soil sample S2 mixed with 0.7% nano-copper. (a) FESEM micrographs and corresponding EDX spectra of elements in S2 soil sample with 0.7% nano-copper. (b) EDX for spectrum which indicate the chemical composition

micrograph shows an occurrence of detrital grains of silt and fine sand fractions and little amount of clay as a matrix between the detrital grains. The specimen has silt-fine sand like structure and characterized by an open fabric system and occurrence of relatively large voids distributed in the specimen. Figure 7.27c, d shows the SEM-micrograph of natural, untreated soil S2 which indicates the sheet-like structure and flaky arrangement of the clay particles. Figure 7.27e, f illustrates the micrograph of natural, untreated soil S3 which shows flaky arrangements of clay particles as matrix between the detrital fine grains. Also the micrograph of untreated soft soil exhibits a fairly open type of microstructure with the platy clay particles assembled in a dispersed arrangement.

Figure 7.28 illustrates the microstructure of S2 soil mixed with 0.7% nano-copper showing the distribution of the nanomaterial in the soil sample. This image was obtained using a Field Emission Scanning Electron Microscope (FESEM) with an energy-dispersive X-ray (EDX) analysis capability. EDX revealed the energy spectrum of the X-ray character emitted from the element of copper (Cu), oxygen (O), silicon (Si), and aluminum (Al). The percentage of all elements were found in the following order: $Cu > O > Si > Al$ (Fig. 4.7b). Copper and oxygen contents were high and widely distributed in soil. Silicon and aluminum were also found in the soil sample, but significantly lower in the constructions. These showed that the mineral composition of the soils in the study areas were CuO , SiO_2 , and Al_2O_3 . The distribution of the nanomaterials after mixing in soil samples can be seen in Fig. 7.29. Figure 7.30a, b, c, d shows the micrographs of nano-magnesium treated soft soil specimens. There is a sign of reticulation and the flocculated nature of the structure becomes more evident, with treated clay particle clusters interspersed with large openings and the clay particles were being coated and bound by the



(a) Sample S1 mixed with 0.5% nano-copper

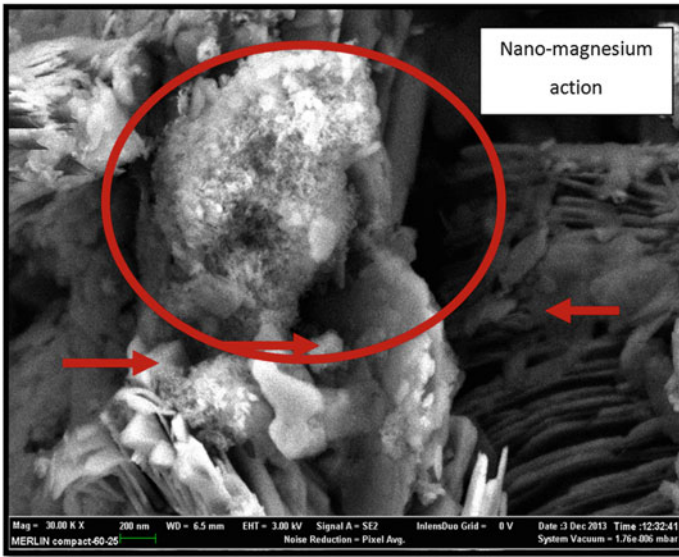


(b) Sample S3 mixed with 0.3% nano-copper

Fig. 7.29 FESEM micrograph of soil samples mixed with nano-copper. (a) Sample S1 mixed with 0.5 % nano-copper. (b) Sample S3 mixed with 0.3 % nano-copper

magnesium gel, which appear as a kind of spongy gel. At the same time, the particle cluster of the structure becomes less evident and degree of reticulation appears to increase. The increase in the degree of reticulation can be attributed to the chemical

(a) FESEM micrograph of S2 with 0.3% nano-magnesium



(b) The spongy gel of nano-magnesium

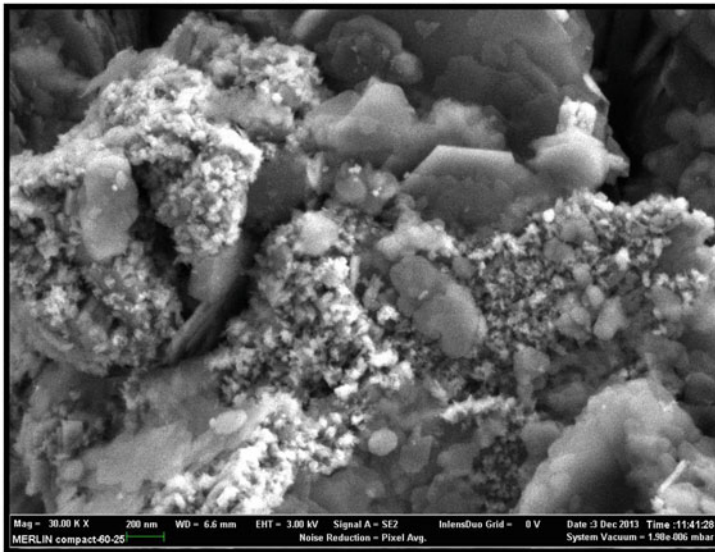
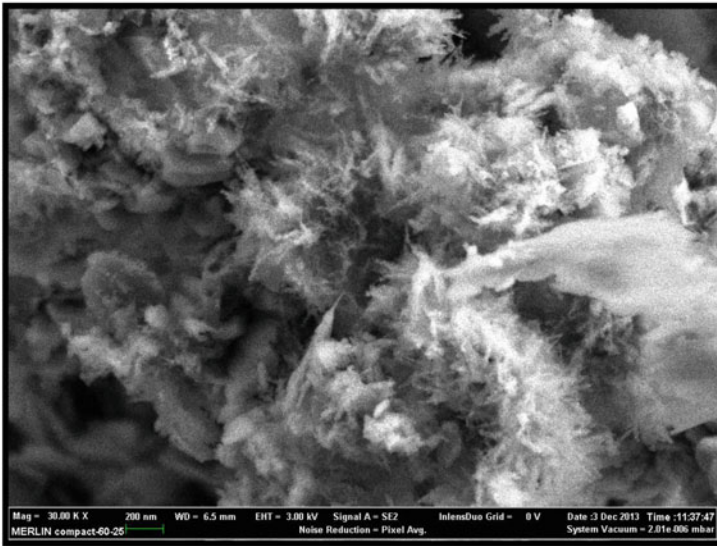


Fig. 7.30 FESEM images of S3 and S2 soil samples treated with nano-magnesium and its chemical action. (a) FESEM micrograph of S2 with 0.3 % nano-magnesium. (b) The spongy gel of nano-magnesium. (c) FESEM micrograph of S3 with 0.3 % nano-magnesium. (d) The nano-magnesium action with S3

(c) FESEM micrograph of S3 with 0.3% nano-magnesium



(d) The nano-magnesium action with S3

Fig. 7.30 (continued)

action of the nano-magnesium. This is consistent with the results of the FT-IR analyses discussed above. As shown in Fig. 7.31a, b, c, d, the soil–nano-alumina mixtures micrographs illustrate the new phase consists of an interlocking network of needle like crystals. Subsequently, bridges were formed between adjacent soil particles. These interlocking networks of needle like crystals have grown into the interstices to form a continuous network. This will be further explained in terms of improvement of strength as well as compressibility behavior in later sections.

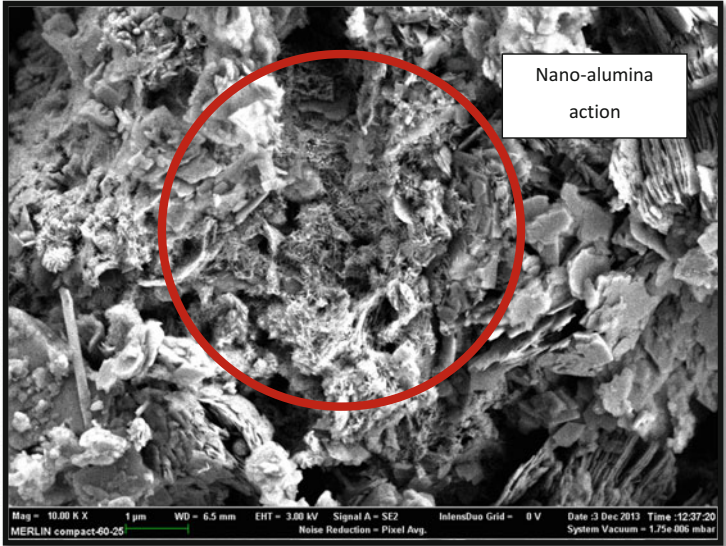
7.7 Effect of Nanomaterials on the Engineering Properties of the Soils

7.7.1 Atterberg Limits

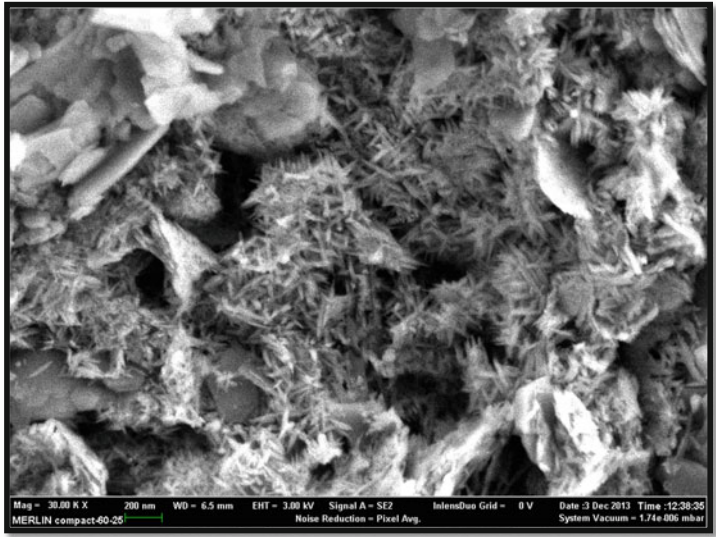
Atterberg limits (Plastic limit “PL,” Liquid limit “LL,” and Plasticity index “PI” = LL-PL) play an important role in soil identification and classification. These parameters indicate to some of the geotechnical problems such as swell potential and workability.

The results of the liquid limit test of the soil samples containing various percentages of nano-copper, nano-alumina, and nano-magnesium used are shown

in Figs. 7.32, 7.33, and 7.34, respectively. The results indicate that for all three soils, the liquid limit decreases with increasing nano-copper, nano-alumina, and nano-magnesium contents especially at optimum nanomaterials contains.

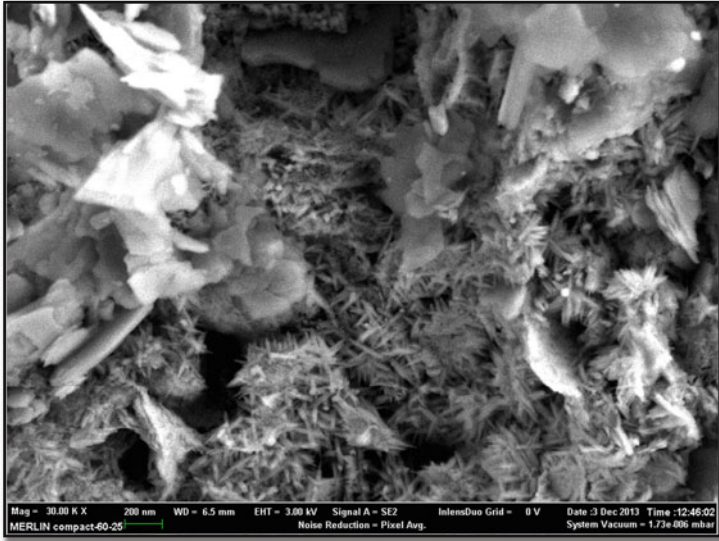


(a) FESEM micrograph of S2 with 0.1% nano-alumina

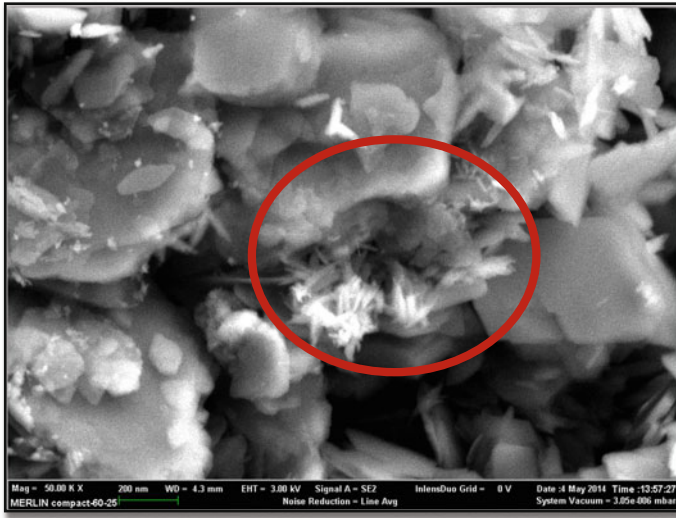


(b) Needle like crystals from the chemical action of nano-alumina

Fig. 7.31 FESEM micrograph of S2 and S3 soil samples treated with nano-alumina. (a) FESEM micrograph of S2 with 0.1 % nano-alumina. (b) Needle like crystals from the chemical action of nano-alumina. (c) FESEM micrograph of S3 with 0.1 % nano-alumina. (d) The nano-alumina action with S3



(c) FESEM micrograph of S3 with 0.1% nano-alumina



(d) The nano-alumina action with S3

Fig. 7.31 (continued)

These decreases are obviously due to the change in water content resulting from increasing nanomaterial content. Nanomaterial particles are believed to coat the clay clast, binding them together and filling the clay matrix, thus reducing the voids and the water contained in the voids (Taha and Taha 2012) (Fig. 7.35).

Fig. 7.32 Effects of nano-copper on the liquid limits

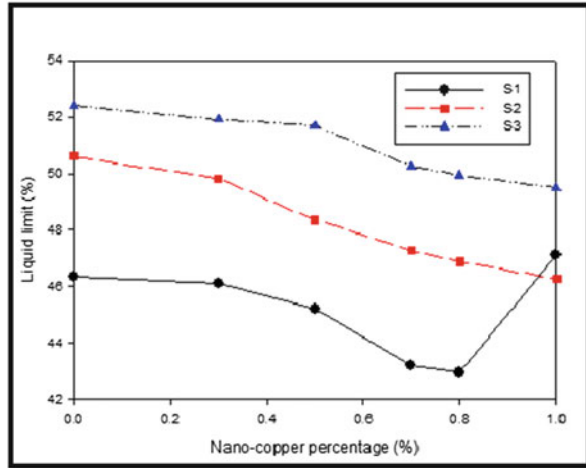
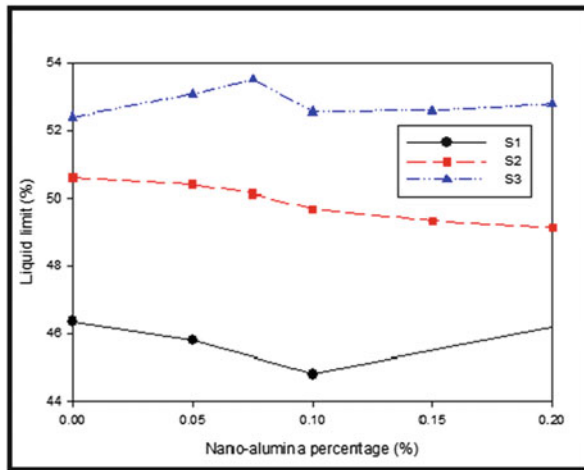


Fig. 7.33 Effects of nano-alumina on the liquid limits



Reductions in the plasticity (Figs. 7.36, 7.37, and 7.38) indices are indicators of soil improvement, because the plasticity index represents the range of water content over which a soil is plastic (Raj 1995). Soils with a high PI may be difficult to work with in construction because of their instability and stickiness when wet. High PI soils also have potential for detrimental volume changes during wetting and drying. Thus, addition of nanomaterials to soil even at low doses can enhance its geotechnical properties. The addition of nano-alumina and nano-magnesium causes some decreases in the plasticity index while an increase in nano-copper content gives a higher decrease in the plasticity index. This is due to the higher density of the nano-alumina, nano-magnesium, and nano-copper particles compared to that of clay

Fig. 7.34 Effects of nano-magnesium on the liquid limits

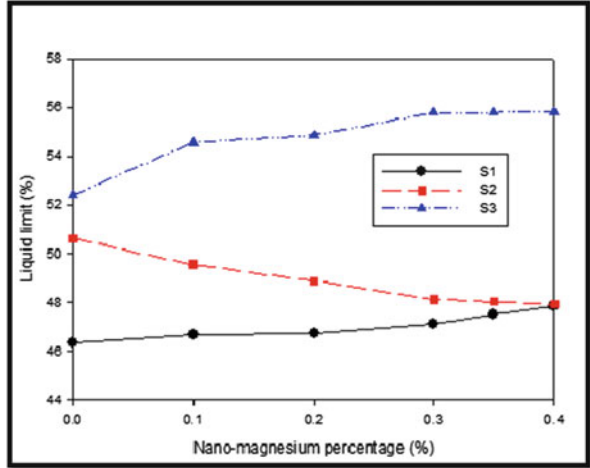
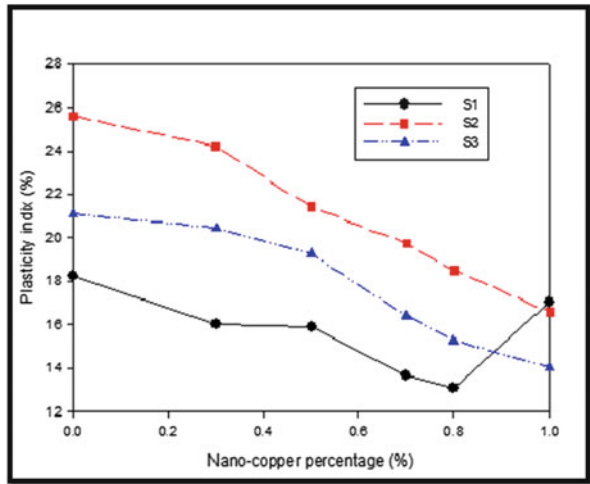


Fig. 7.35 Effects of nano-copper on the plasticity index



particles. Moreover, due to the low content of nano-alumina used with the soil, a slight decrease in plasticity index was observed. However, the reduction in plasticity index is more significant when nano-copper was used due to the high density of nano-copper particle. However, the reduction in plasticity index is more significant for soils with high plasticity index S2 and S3, and especially when nano-copper was used due to the high density of nano-copper particles.

However, the maximum reduction in plasticity index (Fig. 7.38) was noted at 1 % nano-copper content for all types of soils. The reduction in the plasticity index for soil sample S1, S2, and S3 were 1.19, 9.01, and 7.06, respectively, after adding 1 % nano-copper. The reduction in the plasticity index for soil sample S1 was 1.98

Fig. 7.36 Effects of nano-alumina on the plasticity index

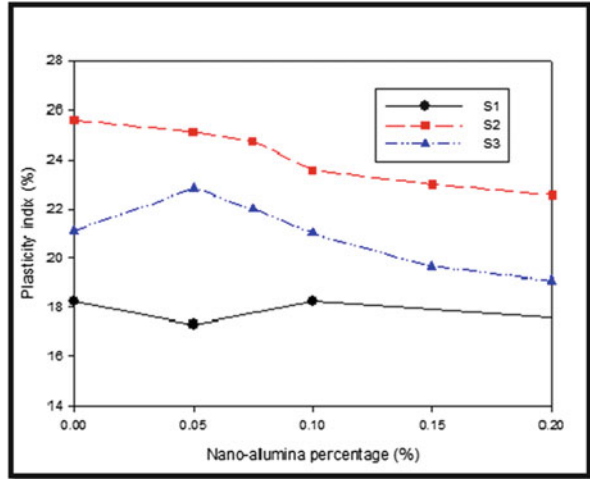
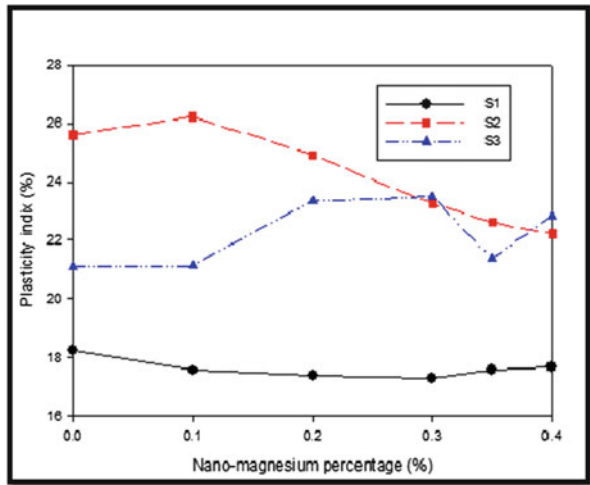
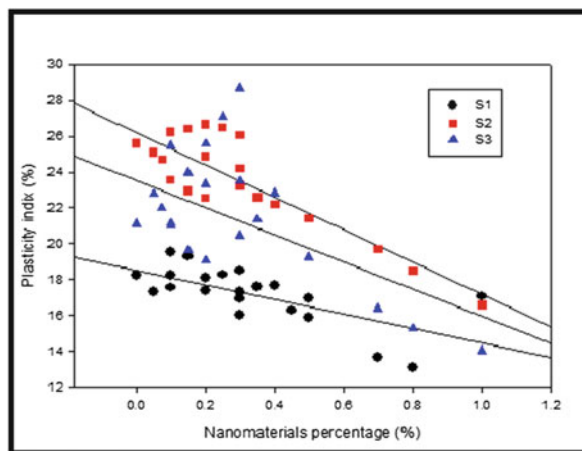


Fig. 7.37 Effects of nanomaterials on the plasticity index



and 0.94 after adding 0.45 % nano-alumina and 0.30 % nano-magnesium, respectively. There was also a reduction in plasticity index for soil sample S2 in which after adding 0.2 % nano-alumina and 0.4 % nano-magnesium, the PI reduced to 3.06 and 3.4, respectively. The reduction in the plasticity index for soil sample S3 was 2.02 after adding 0.2 % nano-alumina.

Fig. 7.38 Effects of nanomaterials on the plasticity index tested soils



7.8 Conclusion

The following conclusions are derived from the findings of this study:

1. Evidence from the FT-IR and SEM analyses has shown that the new phase consists of chemical action of the nanomaterials treatment. The success of the treatment process is dependent on the available nanomaterials content, curing time, soil type, soil pH, and clay minerals.
2. The plasticity index exhibits a significant reduction compared with the untreated soil. This reduction is in proportion with and nanomaterials surface area as well as the doses of nanomaterials.

References

- Akhnouk AK (2013) Overview of nanotechnology applications in construction industry in the united states. *Micro Nanosyst* 5:147–153
- Amorim CLG, Lopes RT, Barroso RC, Queiroz JC, Alves DB, Perez CA, Schelin HR (2007) Effect of clay–water interactions on clay swelling by X-ray diffraction. *Nucl Inst Methods Phys Res A* 580:768–770. doi:[10.1016/j.nima.2007.05.103](https://doi.org/10.1016/j.nima.2007.05.103)
- Bertaux J, Fröhlich F, Ildefonse P (1998) Multicomponent analysis of FTIR spectra: quantification of amorphous and crystallized mineral phases in synthetic and natural sediments. *J Sediment Res* 68:440–447
- Bhushan B (2007) *Springer handbook of nanotechnology*. Springer, New York
- Brar S, Verma M, Tyagi R, Surampalli R (2009) Nanoparticles. *Contamin Emerg Environ Concern* 416–445. doi:[10.1061/9780784410141.ch11](https://doi.org/10.1061/9780784410141.ch11)
- Calik U, Sadoglu E (2014) Classification, shear strength, and durability of expansive clayey soil stabilized with lime and perlite. *Nat Hazards* 71:1289–1303

- Du C, Linker R, Shaviv A (2008) Identification of agricultural Mediterranean soils using mid-infrared photoacoustic spectroscopy. *Geoderma* 143:85–90. doi:[10.1016/j.geoderma.2007.10.012](https://doi.org/10.1016/j.geoderma.2007.10.012)
- Falvo M, Superfine R (2000) Mechanics and friction at the nanometer scale. *J Nanopart Res* 2:237–248
- Givi AN, Abdul Rashid S, Aziz FNA, Mohd Salleh MA (2011) Particle size effect on the permeability properties of nano-SiO₂ blended Portland cement concrete. *J Compos Mater* 45:1173–1180
- Gritco A, Moldovan M, Grecu R, Simon V (2005) Thermal and infrared analyses of aluminosilicate glass systems for dental implants. *J Optoelectron Adv Mater* 7:2845–2847
- Hosseini P, Booshehrian A, Farshchi S (2010) Influence of nano-SiO₂ addition on microstructure and mechanical properties of cement mortars for ferrocement.
- Kempfert H-G, Gebreselassie B (2006) *Excavations and foundations in soft soils*. Springer, Berlin
- Lee J, Mahendra S, Alvarez PJJ (2010) Nanomaterials in the construction industry: a review of their applications and environmental health and safety considerations. *ACS Nano* 4:3580–3590
- Manoharan C, Sutharsan P, Dhanapandian S, Venkatachalapathy R (2012) Spectroscopic and thermal analysis of red clay for industrial applications from Tamilnadu, India. *J Mol Struct* 1027:99–103. doi:[10.1016/j.molstruc.2012.05.079](https://doi.org/10.1016/j.molstruc.2012.05.079)
- Mercier JP, Zambelli G, Kurz W (2002) *Introduction to materials science*. Elsevier Science, Kidington
- Millogo Y, Hajjaji M, Ouedraogo R, Gomina M (2008) Cement-lateritic gravels mixtures: microstructure and strength characteristics. *Construct Build Mater* 22:2078–2086. doi:[10.1016/j.conbuildmat.2007.07.019](https://doi.org/10.1016/j.conbuildmat.2007.07.019)
- Mo L, Deng M, Wang A (2012) Effects of MgO-based expansive additive on compensating the shrinkage of cement paste under non-wet curing conditions. *Cem Concr Compos* 34:377–383. doi:[10.1016/j.cemconcomp.2011.11.018](https://doi.org/10.1016/j.cemconcomp.2011.11.018)
- Montesh G (2005) Swelling-shrinkage measurements of bentonite using coupled environmental scanning electron microscopy and digital image analysis. *J Colloid Interface Sci* 284:271–277
- Montesh G, Duplay J, Martinez L, Mendoza C (2003) Swelling-shrinkage kinetics of Mx80 bentonite. *Appl Clay Sci* 22:279–293
- Muhunthan B, Sariosseiri F, WSDOT Research and Library Services (2008) Interpretation of geotechnical properties of cement treated soils. Washington State Department of Transportation, Office of Research and Library Services
- Olga SSK, Hanna D (2014) Nanotechnology based thermosets. *Handbook of thermoset plastics*, 3rd edn. Elsevier, Amsterdam, pp 623–695
- Pacheco-Torgal F, Jalali S (2011) Nanotechnology: advantages and drawbacks in the field of construction and building materials. *Construct Build Mater* 25:582–590
- Poole CP, Owens FJ (2003) *Introduction to nanotechnology*. Wiley, Hoboken
- Prasad R (2014) Synthesis of silver nanoparticles in photosynthetic plants. *J Nanopart Article ID* 963961. doi:[10.1155/2014/963961](https://doi.org/10.1155/2014/963961)
- Prasad R, Kumar V, Prasad KS (2014) Nanotechnology in sustainable agriculture: present concerns and future aspects. *Afr J Biotechnol* 13:705–713
- Prasad R, Pandey R, Barman I (2016) Engineering tailored nanoparticles with microbes: quo vadis. *WIREs Nanomed Nanobiotechnol* 8:316–330
- Rahmat MN, Kinuthia JM (2011) Effects of mellowing sulfate-bearing clay soil stabilized with wastepaper sludge ash for road construction. *Eng Geol* 117:170–179
- Raj PP (1995) *Geotechnical engineering*. Tata McGraw-Hill, New Delhi
- Sariosseiri F, Muhunthan B (2009) Effect of cement treatment on geotechnical properties of some Washington State soils. *Eng Geol* 104:119–125
- Shand MA (2006) *The chemistry and technology of magnesia*. Wiley, New York
- Sobolev K, Gutiérrez MF (2005) How nanotechnology can change the concrete world. *Am Ceram Soc Bull* 84:14–18

- Sobolev K, Sanchez F (2012) The application of nanoparticles to improve the performance of concrete. Anjuran American Concrete Institute, ACI. Agios Nikolaos, Crete
- Sobolev K, Flores I, Hermosillo R, Torres-Martinez L (2008) Nanomaterials and nanotechnology for high-performance cement composites, vol 254. ACI Special Publication, American Concrete Institute, pp 93–120
- Taha M, Taha O (2012) Influence of nano-material on the expansive and shrinkage soil behavior. *J Nanopart Res* 14:1–13. doi:[10.1007/s11051-012-1190-0](https://doi.org/10.1007/s11051-012-1190-0)
- Ubertini F, Materazzi AL, D'Alessandro A, Laflamme S (2014) Natural frequencies identification of a reinforced concrete beam using carbon nanotube cement-based sensors. *Eng Struct* 60:265–275
- Zhang T, Cheeseman CR, Vandeperre LJ (2011) Development of low pH cement systems forming magnesium silicate hydrate (M-S-H). *Cem Concr Res* 41:439–442. doi:[10.1016/j.cemconres.2011.01.016](https://doi.org/10.1016/j.cemconres.2011.01.016)